RESEARCH ARTICLE

Editorial Process: Submission:07/09/2025 Acceptance:03/27/2026 Published:04/07/2026

In Silico Identification of Hydroxyxanthone Derivatives as CDK2/EGFR Dual Inhibitor for Colorectal Cancer Treatment

Faris Hermawan[1], Anita Dwi Puspitasari[2]*, Lala Adetia Marlina[3], Ervan Yudha[4], Nela Fatmasari[5], Lathifah Puji Hastuti[6], Rissa Laila Vifta[7]

Abstract

Objective: Both CDK2 (cyclin-dependent kinase 2) and EGFR (epidermal growth factor receptor) play significant roles in the development and progression of colorectal cancer. In vitro studies of several hydroxyxanthone derivatives for the treatment of WiDr cancer cell lines have revealed potential anticancer activity against colorectal cancer. The present study aims to identify hydroxyxanthone derivatives as potential drug candidates for colorectal cancer treatment through an in silico approach. **Methods:** Interactions between seven hydroxyxanthone (X1–X7) derivatives and CDK2 and EGFR were analyzed using molecular docking, molecular dynamics simulations, and binding energy calculations based on the MM-PBSA method. We also evaluated the physicochemical properties and ADMET profiles using the pkCSM server. **Result:** Docking studies demonstrated that all hydroxyxanthone derivatives exhibited favorable binding affinities, ranging from –7.25 to –8.57 kcal/mol against CDK2 and –6.79 to –8.31 kcal/mol against EGFR. Following 200 ns molecular dynamics simulations, compounds X4, X5, and X7 showed higher structural stability than doxorubicin and comparable stability to the native ligands C62 and erlotinib. Consistently, MM/PBSA analysis revealed that X4 (–20.27 kcal/mol) and X7 (–25.29 kcal/mol) achieved the most favorable binding free energies for CDK2 and EGFR, respectively. Moreover, these compounds satisfied Lipinski's criteria and met the minimum requirements for ADMET drug-likeness parameters. **Conclusion:** Hydroxyxanthone derivatives X4, X5, and X7 exhibit the strongest potential as dual CDK2/EGFR inhibitors and may, therefore, serve as promising candidates for colorectal cancer therapy. Nevertheless, further in vitro and in vivo investigations are required to experimentally validate their therapeutic potential.

Keywords: Hydroxyxanthone- molecular dynamics- molecular docking- tyrosine kinase

Asian Pac J Cancer Prev, **27 (4)**, 1265-1276

Introduction

Cancer is the second leading cause of death, following cardiovascular illnesses. In 2020, there were almost 19.3 million new diagnoses of cancer and nearly 10 million deaths due to cancer [1]. Colorectal cancer is the third most frequent and second deadliest cancer worldwide [2]. In 2018, there were approximately 1.8 million new cases of CRC, resulting in 0.9 million deaths. Early detection of colorectal cancer increases 5-year survival to 90%. However, if patients have distant metastasis at diagnosis, the 5-year survival rate reduces to just 10% [3]. Therefore, there is no reason not to make significant efforts to decrease the number of active cases of colorectal cancer and its rate of mortality in the coming years.

Several standard chemotherapy drugs used to cure and treat colorectal cancer have been made commercially available worldwide. Common chemotherapy medicines, such as doxorubicin, can potentially be utilized for the treatment of colorectal cancer; however, they suffer from limited targeting and low selectivity [4]. As a result, there is an increasing interest in discovering novel anticancer drugs to address this issue.

Cancer growth is a complex series of events involving cell growth, blood vessel formation, invasion, and spread to other parts of the human body [5]. Extensive networks of communication inside cells regulate these processes. Mutations in these pathways, including those affecting cyclin-dependent kinases (CDK2/Cyclins), can stimulate the rapid growth of cancer cells [6]. CDK2 mainly engages with cyclins A, B, and E, playing a crucial role in regulating the cell cycle. The G1 to S phase transition

*[1]Research Center for Pharmaceutical Ingredients and Traditional Medicine, National Research and Innovation Agency (BRIN), Tangerang Selatan, Banten 15314, Indonesia. [2]Faculty of Pharmacy, Universitas Wahid Hasyim, Semarang 50236, Indonesia. [3]Research Center for Computing, National Research and Innovation Agency (BRIN), Cibinong, Bogor 16911, Indonesia. [4]Department of Chemistry, Faculty of Mathematics and Natural Sciences, Universitas Gadjah Mada, Yogyakarta 55281, Indonesia. [5]Chemistry Education, Sultan Ageng Tirtayasa University, Serang, Banten 42117, Indonesia. [6]Graduate School, Universitas Padjadjaran, Bandung 45363, Indonesia. [7]Faculty of Pharmacy, Universitas Islam Sultan Agung, Semarang 50112, Indonesia. *For Correspondence: anita@unwahas.ac.id*

in the cell cycle of cells is responsible for this. CDK2 plays a crucial role in the proliferation and advancement of cancer cells [7]. Furthermore, three colon cancer cell lines, DLD-1 HCT116, and HCT15, demonstrate significantly elevated expression of CDK2 relative to "normal" human colon epithelial cells. This suggested that CDK2 could serve as a potential therapeutic target for colon cancer therapy [8].

The function of the epidermal growth factor receptor (EGFR) in cancer growth and survival is frequently underestimated [9]. The EGFR is a tyrosine kinase receptor from the ErbB protein family. Ligand binding to the tyrosine kinase domain stimulates signaling pathways that regulate cell proliferation, angiogenesis, survival, migration, and adhesion. Considering that these pathways are vital for the survival of cancer cells, EGFR is a key target in the treatment of colorectal carcinoma metastases [10]. Inhibiting these protein receptors prevents cancer cells from spreading and growing in number, causing cancer cell death. This mechanism provides valuable insight into the design and development of novel colorectal anticancer pharmaceuticals that will eventually replace doxorubicin.

Hundreds of chemotherapy drugs have been developed and produced in the last few years [11, 12]. Among them, xanthone derivatives have demonstrated potential anticancer action in vitro, in vivo, and even in clinical studies [13]. The xanthone has a simple chemical structure and may associate with various protein receptors, providing a broad range of anticancer agents based on the position, number, and type of the attached functional groups. QSAR analysis on several hydroxy group substituted xanthone derivatives obtained IC_{50} predictions against WiDr cells ranging from 0.011 to 5.498 μM [14]. The in vitro study of hydroxyxanthone derivatives in treating WiDr, MCF7, and HepG2 cancer cells revealed that the addition of one hydroxyl group increased the potency of the anticancer activity [15, 16]. There is currently no published information on molecular docking, molecular dynamics simulation, or MM-PBSA binding energy calculations for xanthone derivatives with hydroxy and other alkoxy functional groups. The aim of this study was to investigate seven hydroxyxantone derivatives to determine their inhibitory mechanisms, interactions, and stability towards the active sites of CDK2 and EGFR proteins. The experiment consisted of molecular docking study, molecular dynamics simulation, bond energy calculation by MM-PBSA method, and ADMET prediction.

Materials and Methods

Material

The protein tyrosine kinases, i.e., CDK2 and EGFR, were obtained from the RSCB Protein Data Bank database (www.rcsb.org) with the PDB ID of 2UZO and 1M17, respectively. Subsequently, a series of hydroxyxanthone derivatives (X1-X7) was used as ligands for an in silico study, and their chemical structures are displayed in Figure 1.

Molecular Docking

Two protein tyrosine kinases (CDK2, EGFR) were prepared using chimera software. The protein and ligand were first separated from water molecules. Subsequently, both structures were optimized using UCSF Chimera by adding hydrogen atoms, assigning appropriate charges, and completing any missing side chains. The optimized structures were then saved in PDB format for docking analysis [17]. Subsequently, the three-dimensional structures of the hydroxyxanthone derivatives (X1–X7) were constructed using the Avogadro software and subsequently subjected to geometric optimization with the ORCA program employing the DFT B3LYP/3-21G

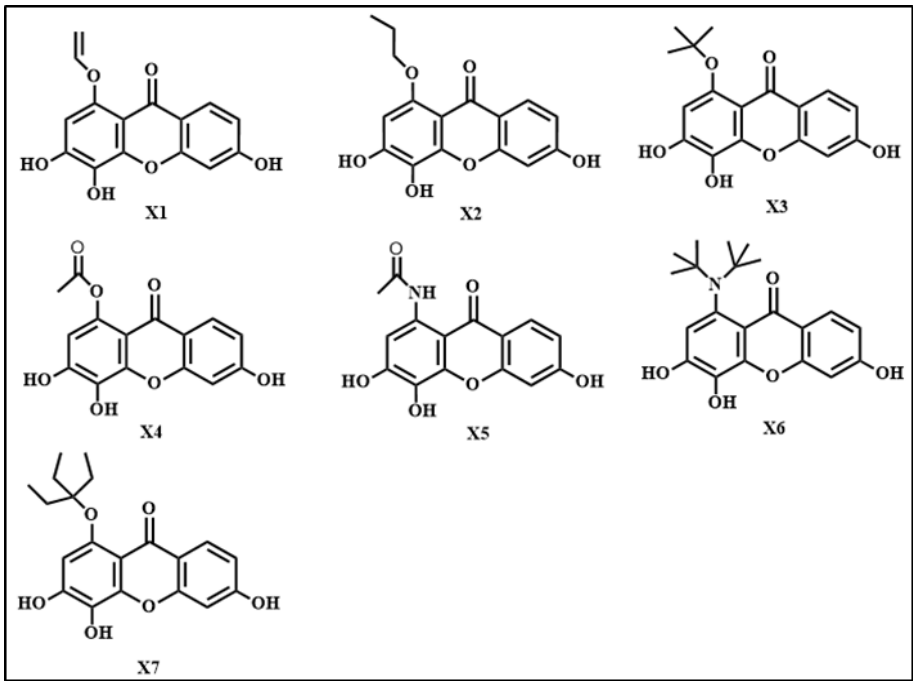

Figure 1. The Structure of Hydroxyxanthone Derivatives X1-X7

method [18, 19]. The optimized structures were saved in the PDB format. The molecular docking study of hydroxyxanthone derivatives started with the redocking process. AutoDock4 software was used for redocking and docking analysis of EGFR and PDGFR proteins in 42×40×40 Å and 40×40×50 Å grid boxes, respectively [20, 21]. The Lamarckian Genetic Algorithm (LGA) was employed for 50 iterations, and the 2D interaction structure resulting from molecular docking was visualized using Discovery Studio Visualizer (DSV) [22, 23].

Molecular Dynamics Simulation

Molecular Dynamics (MD) simulation was generated utilizing the GROMACS 2020 program [24]. Topology proteins CDK2 and EGFR were created using the charmm36 force for performing MD simulations [25]. The topology parameters of hydroxyxanthones were completed utilizing the cgenff server (cgenff.com) [26]. In these MD simulations, periodic boundary conditions (PBC) were utilized as a small representation of the real system, which in this system used a cubic unit cell shape. Subsequently, the energy minimization was performed with the steepest descent for 1 ns; minimization was terminated when the energy reached 10 kJ/mol. Equilibration was performed using the NVT and NPT systems with system conditions for 1 ns each with dt 2 fs at 300 K and 1 atm. System conditions were controlled as isotropic, PME (Particle Mesh Ewald) for long-range electrostatic, and v-rescale of modified Berendsen thermostat were conducted for temperature coupling [27-29]. MD Production of hydroxyxanthones against CDK2 and EGFR proteins was conducted for 200 ns under the same conditions. The results of a 200-ns MD simulation, including Root Mean Square Deviation (RMSD), Root Mean Square Fluctuation (RMSF), Radius of Gyration (Rg), and Hydrogen Bond (H-bond).

Calculation of MM-PBSA Energy

The molecular mechanics Poisson-Boltzmann surface area (MM-PBSA) studies were performed to determine free energy, including van der Waals, electrostatic, polar solvation, SASA, and binding energies, during MD simulation. The free binding energies were calculated using the g_mmpbsa program [30]. The ligand-protein MD trajectory data and parameter file were utilized to run the g_mmpbsa using a single-step calculation.

ADMET prediction

The optimized hydroxyxanthone derivatives structure in PDB format was converted to SMILES format using the Discovery Studio Visualizer [31]. Afterward, those structures were submitted one by one to the pkCSM web server [32]. The physicochemical and ADMET parameters were chosen by selecting the ADMET menu. Subsequently, the pkCSM server gave information data for each compound, including Lipinski's rule of five, absorption, distribution, metabolism, excretion, and toxicity.

Results

Molecular docking of hydroxyxanthones towards the CDK2 protein

The compounds X1-X7 and doxorubicin were docked in the same position with C62 as a native ligand of the CDK2 protein. Table 1 displays the binding energy results between hydroxyxanthones X1-X7, native ligand C62, and doxorubicin with the CDK2 protein. Figure 2 shows the 2D interaction of compound X7, native ligand C62, and doxorubicin against CDK2 protein.

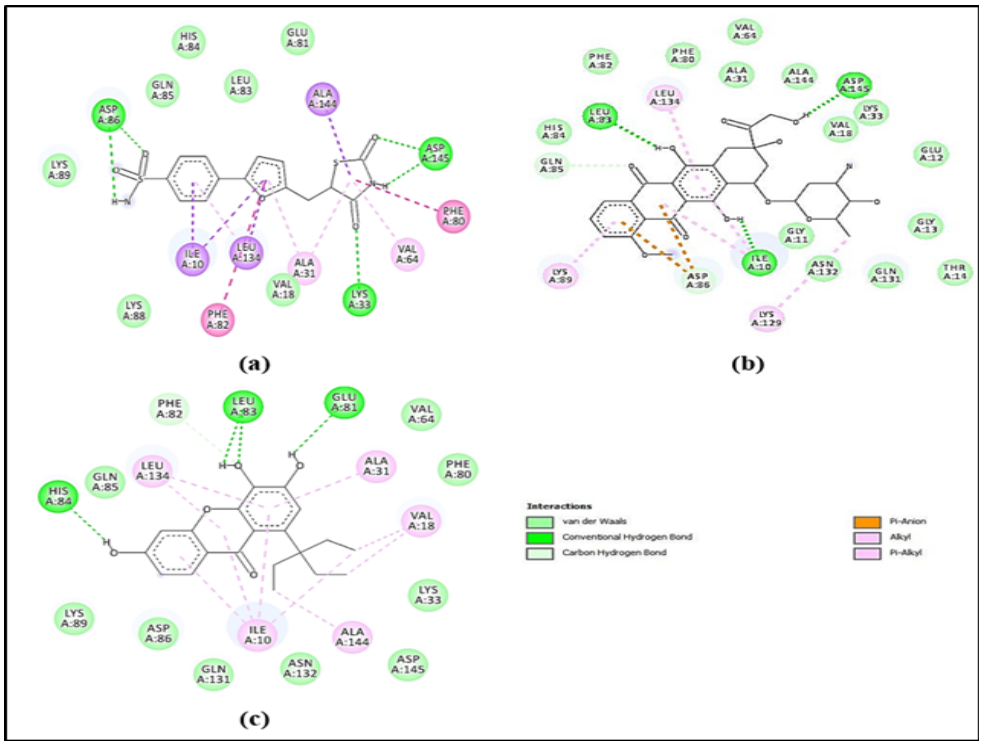

Figure 2. The 2D Interactions of compound (a) ligand C62, (b) doxorubicin, and (c) X7 against CDK2 protein

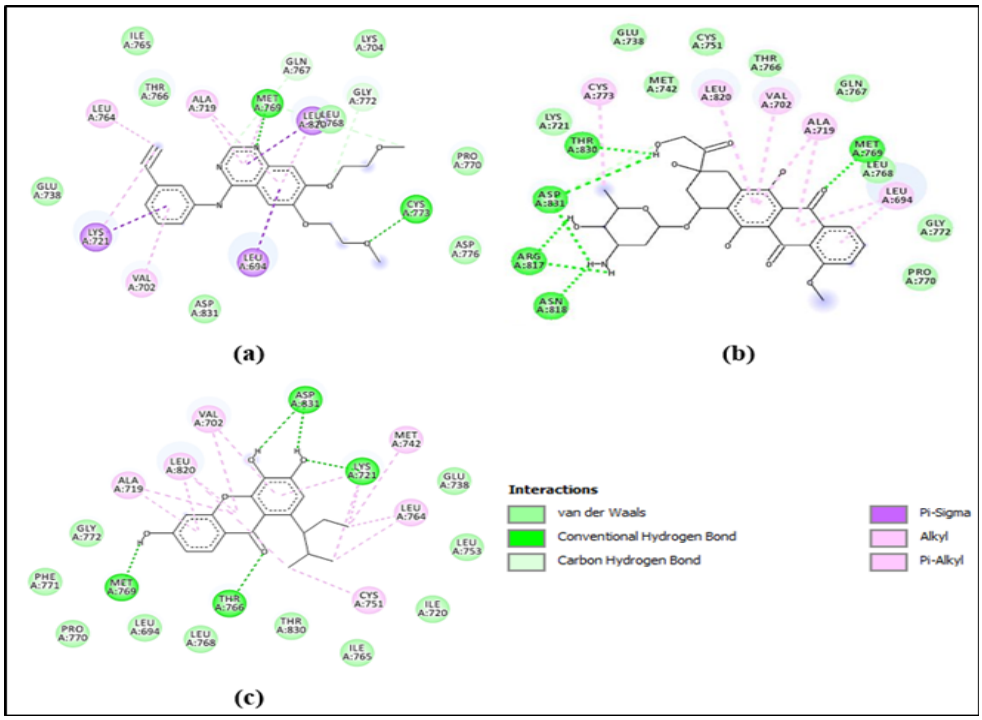

Figure 3. The 2D Interactions of Compound (a) ligand Erlotinib, (b) doxorubicin, and (c) X7 against the EGFR protein

Molecular docking of hydroxyxanthones towards the EGFR protein

The compounds X1-X7 and doxorubicin were docked in the same position as erlotinib, a native ligand of the EGFR protein. Table 2 displays the binding energy results between hydroxyxanthones X1-X7, native ligand erlotinib, and doxorubicin with the EGFR protein. Figure 3

Table 1. The Binding Energy of X1-X7, Ligand C62, Doxorubicin against CDK2 Protein

Compound	Binding Energy (kcal/mol)	H-bond
X1	-7.25	His84, Leu83, Glu81
X2	-7.26	His84, Leu83, Glu81, Asp86
X3	-8.14	His84, Leu83, Glu81
X4	-7.87	His84, Leu83, Glu81, Lys33
X5	-7.41	His84, Leu83, Glu81, Lys33, Asp86
X6	-7.97	His84, Leu83, Glu81
X7	-8.57	His84, Leu83, Glu81
C62	-9.49	Asp86, Asp145, Lys33
Doxorubicin	-7.84	Leu83, Asp145, Ile10

Table 2. The Binding Energy of X1-X7, Ligand Erlotinib, and Doxorubicin against the EGFR Protein

Compound	Binding Energy (kcal/mol)	H-bond
X1	-7.01	Asp831, Lys721, Thr766, Met769
X2	-7.23	Asp831, Lys721, Thr766, Met769
X3	-7.52	Asp831, Lys721, Met769
X4	-7.17	Asp831, Lys721, Thr766, Met769
X5	-7.29	Asp831, Lys721, Thr766, Met769
X6	-6.79	Asp831, Lys721, Gln767, Met769
X7	-8.31	Asp831, Lys721, Thr766, Met769
Erlotinib	-7.05	Met769, Cys773
Doxorubicin	-10.23	Asn818. Arg817. Asp831. Thr830. Met769

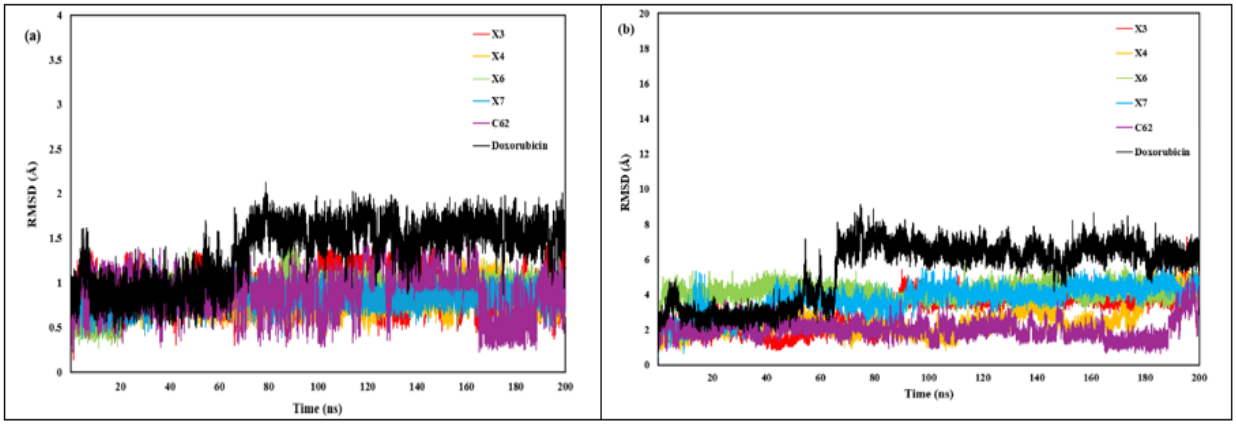

Figure 4. (a) The RMSD ligand and (b) RMSD complex of C62, doxorubicin, and compounds X3, X4, X6, and X7

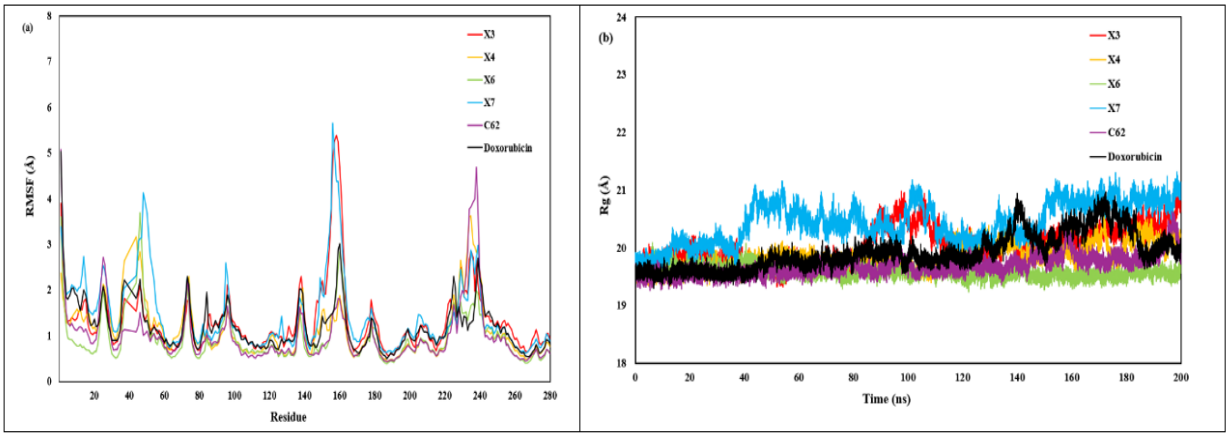

Figure 5. (a) RMSF and (b) Radius of gyration of C62, doxorubicin, and compounds X3, X4, X6, and X7

shows the 2D interaction of compound X7, native ligand erlotinib, and doxorubicin against the EGFR protein.

Molecular dynamics simulation and MM-PBSA binding energy of hydroxyxanthone derivatives toward CDK2 Protein

A 200-ns molecular dynamics simulation was performed involving the native ligand (C62), doxorubicin, and hydroxyxanthones X3, X4, X6, and X7 against the CDK2 protein. The stability of the ligand-protein complex was measured using the root mean square deviation (RMSD) of the ligand and protein complex (Figure 4), the root mean square fluctuation (RMSF) of the simulation system backbone (Figure 5a), the radius of gyration (Rg) (Figure 5b), and the hydrogen bond (Figure 6). Table 3 displays the binding energies of native ligand (C62), doxorubicin, and hydroxyxanthones X3, X4, X6, and X7 during MD simulation by MM-PBSA methodology.

Molecular dynamics simulation and MM-PBSA binding energy of hydroxyxanthone derivatives toward EGFR Protein

A 200-ns molecular dynamics simulation was

Table 3. MM-PBSA Binding Energy of Ligand C62, Doxorubicin, and Compounds X3, X4, X6, and X7 toward CDK2 Protein

Compound	van der Waal's energy (kcal/mol)	Electrostatic energy (kcal/mol)	Polar solvation energy (kcal/mol)	Nonpolar solvation energy (kcal/mol)	Gas-phase free energy (kcal/mol)	Solvation free energy (kcal/mol)	Binding energy (kcal/mol)
X3	-32.90	-13.18	33.64	-3.46	-46.08	30.17	-15.91
X4	-32.77	-31.87	47.79	-3.43	-64.63	44.36	-20.27
X6	-33.73	-15.14	44.36	-4.06	-48.87	40.30	-8.57
X7	-32.74	-7.27	32.78	-3.91	-40.01	28.86	-11.15
C62	-32.57	-39.51	33.08	-3.66	-72.08	29.41	-42.66
Doxorubicin	-33.12	9.92	13.35	-4.45	-23.20	8.90	-14.30

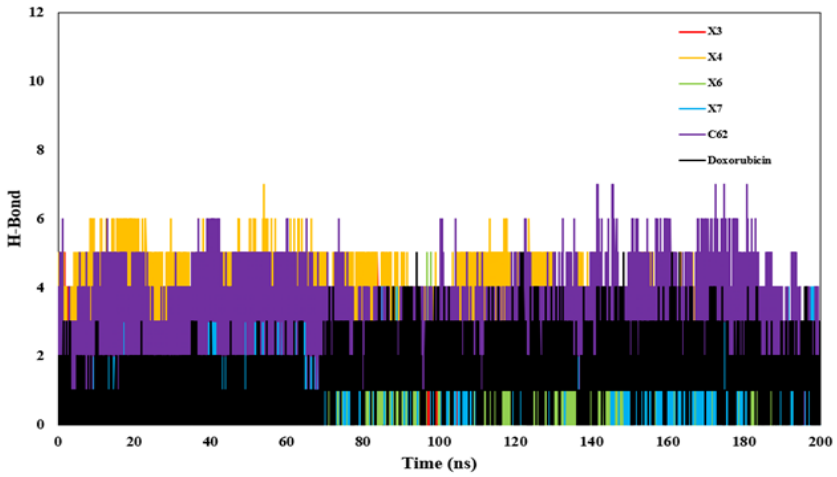

Figure 6. The Hydrogen Bond of Ligand C62, Doxorubicin, and Compounds X3, X4, X6, and X7

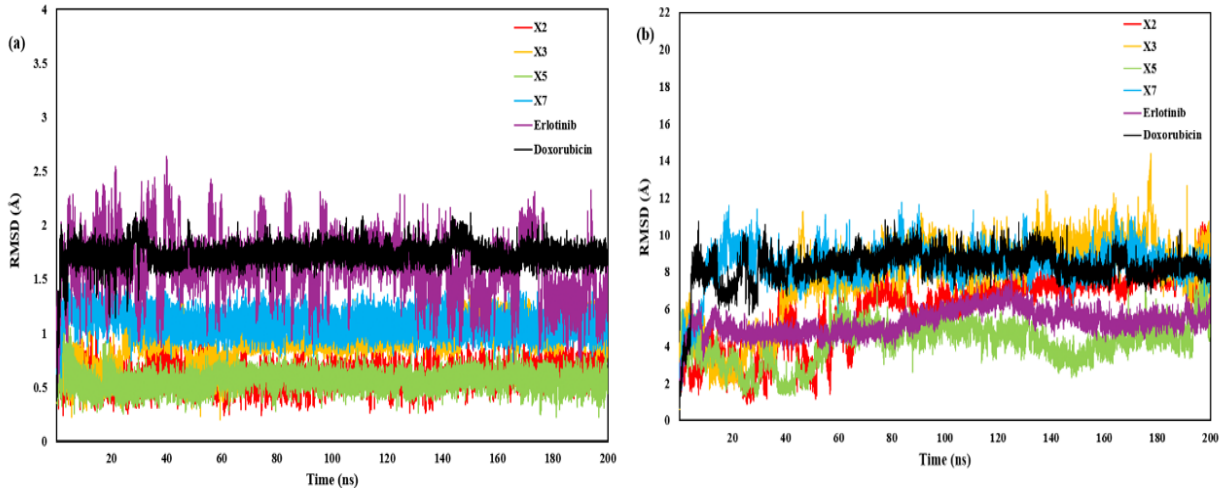

Figure 7. (a) The RMSD ligand and (b) RMSD complex of erlotinib, doxorubicin, and compounds X2, X3, X5, and X7

Table 4. MM-PBSA Binding Energy of Ligand Erlotinib, Doxorubicin, and Compounds X3, X4, X6, and X7

Compound	van der Waal's energy (kcal/mol)	Electrostatic energy (kcal/mol)	Polar solvation energy (kcal/mol)	Nonpolar solvation energy (kcal/mol)	Gas-phase free energy (kcal/mol)	Solvation free energy (kcal/mol)	Binding energy (kcal/mol)
X2	-32.97	-24.92	48.63	-3.67	-57.90	44.97	-12.93
X3	-27.17	-11.06	27.03	-3.30	-38.22	23.73	-14.49
X5	-35.13	-26.25	41.59	-3.35	-61.37	38.24	-23.13
X7	-35.75	-6.81	20.37	-3.77	-42.55	16.60	-25.96
Erlotinib	-40.35	-17.39	30.34	-4.90	-57.74	25.44	-32.30
Doxorubicin	-32.06	-168.62	183.19	-4.35	-200.68	178.84	-21.84

performed involving the native ligand (erlotinib), doxorubicin, and hydroxyxanthones X3, X4, X6, and X7 against the EGFR protein. The stability of the ligand-protein complex was measured using the root mean square deviation (RMSD) of the ligand and protein complex (Figure 7), the root mean square fluctuation (RMSF) of the simulation system backbone (Figure 8a), the radius of gyration (Rg) (Figure 8b), and the hydrogen bond (Figure 9). Table 4 displays the binding energies of native ligand (erlotinib), doxorubicin, and hydroxyxanthones X3, X4, X6, and X7 during MD simulation by MM-PBSA methodology.

Pharmacokinetic Properties of Hydroxyxanthones

Table 5 displays the physicochemical and ADMET data for hydroxyxanthones X2, X3, X5, and X7.

Discussion

Molecular docking studies of hydroxyxanthones X1–X7 were conducted against two types of cancer proteins, namely, CDK2 and EGFR. The docking parameters were

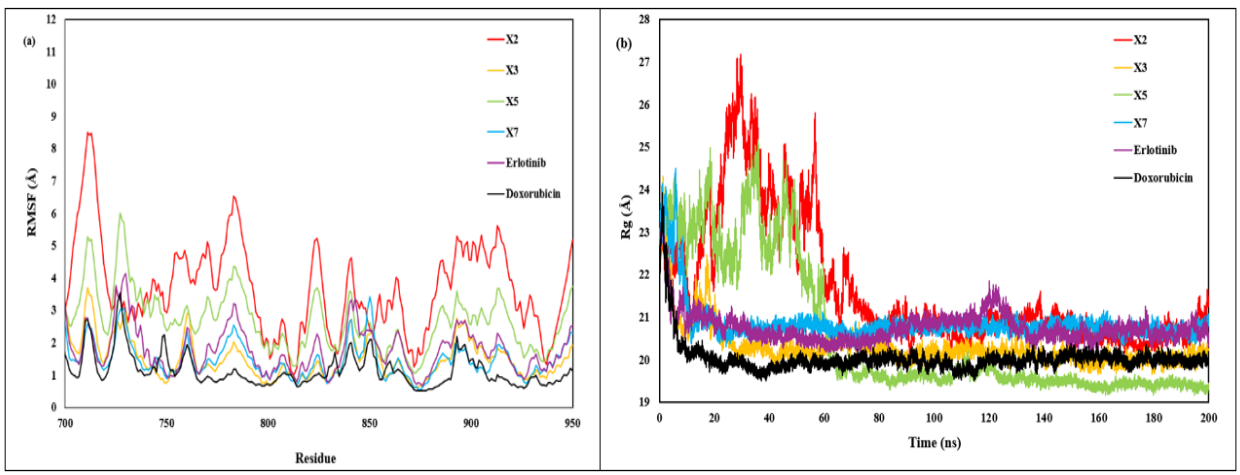

Figure 8. (a) RMSF and (b) Radius of gyration of erlotinib, doxorubicin, and compounds X2, X3, X5, and X7

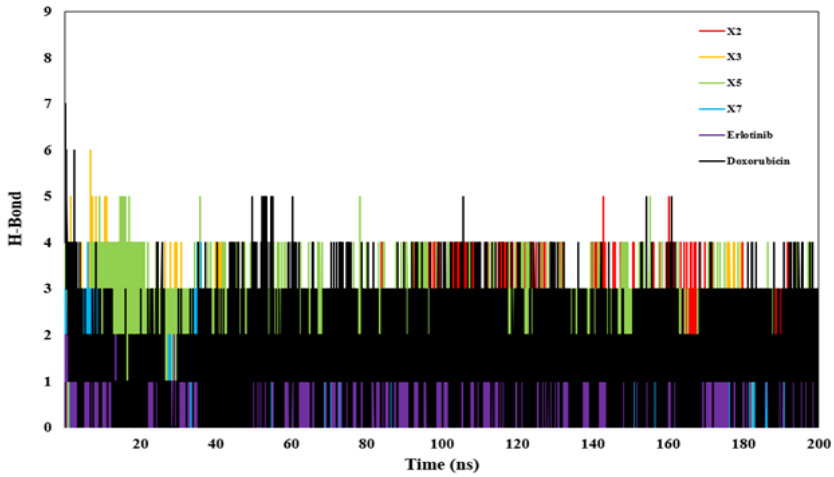

Figure 9. The Hydrogen Bond of Ligand Erlotinib, Doxorubicin, and Compounds X2, X3, X5, and X7

Table 5. Physicochemical and ADMET Properties of Compounds X2, X3, X5, and X7

	Properties	Compound			
		X2	X3	X5	X7
Physicochemical	Molecular weight	302.282	300.31	301.254	342.391
	log P	2.852	3.361	2.021	4.531
	Rotatable bond	3	0	1	4
	H-bond acceptor	6	5	6	5
	H-bond donor	3	3	4	3
	Surface area	124.352	125.604	122.585	144.698
Absorption	CaCO2 permeability	0.027	1.32	-0.317	1.132
	Intestinal absorption	90.799	95.086	85.695	94.49
	Skin permeability	-2.736	-2.735	-2.735	-2.735
Distribution	VDss	0.032	-1.014	-0.249	-0.643
	BBB permeability	-1.12	-0.973	-1.422	-1.147
	CNS permeability	-2.414	-1.887	-2.649	-2.018
Metabolism	CYP2D6 substrate	No	No	No	No
	CYP3A4 substrate	No	No	No	No
	CYP2D6 inhibitor	No	No	No	No
	CYP3A4 inhibitor	No	No	No	No
Excretion	Total clearance	0.251	0.039	0.357	0.334
	Renal OCT2 substrate	No	No	No	No
Toxicity	AMES Toxicity	Yes	Yes	Yes	Yes
	Max. Tolerated dose	0.818	0.564	0.843	0.667
	hERG I inhibitor	No	No	No	No
	hERG II inhibitor	Yes	Yes	Yes	Yes
	Hepatoxicity	No	No	Yes	Yes
	Skin sensitization	No	No	No	No

validated in the initial docking step through a redocking process. The redocking results revealed that ligand C62 had a binding energy of -9.49 kcal/mol and an RMSD of 1.52 Å. Meanwhile, erlotinib had a binding energy of -7.05 kcal/mol with an RMSD value of 1.59 Å. These ligands have RMSD values less than 2, demonstrating that the docking parameters were sufficiently accurate for the molecular docking study of hydroxyxanthone derivatives [33, 34].

The binding energy analysis of the hydroxyxanthone derivatives against the CDK2 protein revealed notable differences in their binding affinities, reflecting the influence of structural variations on ligand–protein interactions. Among the tested compounds, X7 exhibited the most favorable binding energy of –8.57 kcal/mol, suggesting the strongest affinity toward the CDK2 active site and a high degree of binding stability. This was followed by X3 (–8.14 kcal/mol) and X6 (–7.97 kcal/

mol), both of which demonstrated strong and stable interactions indicative of effective engagement with key residues within the CDK2 catalytic pocket. Compound X4 (–7.87 kcal/mol) and the standard drug Doxorubicin (–7.84 kcal/mol) showed comparable binding energies, suggesting moderate but meaningful interactions with the target protein. In contrast, X1 (–7.25 kcal/mol), X2 (–7.26 kcal/mol), and X5 (–7.41 kcal/mol) exhibited slightly weaker binding affinities, implying reduced stabilization within the CDK2 binding site. The reference inhibitor C62, with a binding energy of –9.49 kcal/mol, displayed the strongest interaction overall, serving as a benchmark for comparison. Notably, the binding energy of X7 is relatively close to that of the reference compound, indicating that this derivative may possess comparable inhibitory potential.

The molecular docking analysis revealed that all designed compounds (X1–X7) exhibited stable hydrogen bond interactions within the ATP-binding site of CDK2, supported by additional van der Waals, alkyl, π–σ, and π-alkyl interactions (Figure 2). The hydrogen-bonding profiles varied slightly among compounds but consistently involved key residues within the active site. Compounds X1, X3, X6, and X7 established hydrogen bonds primarily with His84, Leu83, and Glu81. Compounds X2 and X4 additionally formed hydrogen bonds with Asp86 and Lys33, residues also engaged by the native ligand C62, while X5 displayed the broadest interaction network involving His84, Leu83, Glu81, Lys33, and Asp86. Subsequently, a native ligand C62 interacted with Asp86, Asp145, and Lys33, while doxorubicin formed hydrogen bonds with Leu83, Asp145, and Ile10 (Table 1). These findings align with crystallographic studies that identified Lys33, Glu51, Phe80, Leu83, and Asp145 as essential residues for CDK2 function and inhibitor recognition [35, 36]. The interactions of critical residues such as Lys33 and Leu83 by the designed compounds, particularly X2, X4, and X5, indicate their potential to emulate the binding features of established CDK2 inhibitors. The consistent hydrogen bonding with Leu83 and His84, located within the hinge region, further supports the structural stability of the complexes. Collectively, these results suggest that the designed ligands, especially X5 and X7, exhibit favorable and specific hydrogen-bonding interactions conducive to potent CDK2 inhibition.

The docking results of the hydroxyxanthone derivatives against the EGFR protein revealed that X7 exhibited the strongest binding affinity (–8.31 kcal/mol), indicating the most stable interaction with the active site. While compound X3 also showed a favorable binding energy (–7.52 kcal/mol), followed by X2, X4, and X5, which demonstrated comparable affinities in the range of –7.17 to –7.29 kcal/mol. In contrast, X1 (–7.01 kcal/mol) and X6 (–6.79 kcal/mol) displayed slightly weaker interactions. The reference inhibitor Erlotinib had a binding energy of –7.05 kcal/mol, suggesting that several derivatives, particularly X7, may possess stronger inhibitory potential. Meanwhile, Doxorubicin showed a markedly higher binding affinity (–10.23 kcal/mol), likely due to its distinct structure and binding mode. Overall, these results identify X7 as the most promising hydroxyxanthone derivative for further evaluation as a potential EGFR inhibitor.

The molecular docking analysis revealed that all designed compounds (X1–X7) formed stable hydrogen bond interactions within the ATP-binding site of EGFR (PDB ID: 1M17). Additional interactions, including van der Waals, alkyl, π–σ, π-alkyl, and carbon–hydrogen bonds, further stabilized the ligand–protein complexes (Figure 3). The predominant hydrogen-bonding residues Asp831, Lys721, Thr766, and Met769 were consistently engaged across most ligands, suggesting a conserved binding orientation. Compounds X1–X5 displayed similar hydrogen-bonding profiles, whereas X6 formed an additional interaction with Gln767, and X7 maintained hydrogen bonds with all four key residues (Table 2). In comparison, the reference inhibitor erlotinib interacted with Met769 and Cys773, while doxorubicin formed broader but less specific hydrogen bonds involving Asn818, Arg817, Asp831, Thr830, and Met769. Previous structural analyses have identified Met769, Glu767, Gly700, Gly695, Tyr845, Gly833, Asp818, Arg812, and Asp831 as essential residues contributing to EGFR inhibition and regulation of cancer cell proliferation [37]. Among these, Met769 represents a critical hinge residue responsible for stabilizing inhibitor binding. The hydrogen-bonding interactions observed in this study, particularly those involving Met769 and Asp831, indicate that all compounds had the key interactions of potent ATP-competitive EGFR inhibitors, underscoring their potential as selective and stable EGFR-targeting candidates.

The ligand to ligand RMSD profiles indicated that all candidate compounds maintained high structural stability throughout the 200 ns molecular dynamics simulation (Figure 4a). Compounds X3, X4, X6, X7, and C62 exhibited RMSD values consistently below 2 Å, demonstrating minimal internal conformational deviations. Although the reference ligand doxorubicin displayed slightly larger fluctuations. The ligand to backbone RMSD trajectories corroborated these findings by revealing that all designed ligands sustained stable positions relative to the CDK2 active site without evidence of significant displacement or partial unbinding (Figure 4b). Doxorubicin showed higher RMSD values, indicating greater mobility and a comparatively less stable binding mode.

The RMSF analysis showed that the CDK2 backbone remained predominantly stable across all ligand-bound systems, including within the binding pocket region spanning residues 18–150 identified from docking (Figure 5a). Moderate fluctuations were restricted to flexible regions, particularly around residues 40–60, 150–170, and 230–245, without affecting the structural integrity of the ligand-binding site. Consistently, the radius of gyration profiles indicated that all complexes retained stable global compactness throughout the 200 ns simulation (Figure 5b). Among the systems, Ligands X3, X4, X6, and C62 promoted slightly higher structural compactness, whereas X7 exhibited modestly increased flexibility but remained structurally stable. The hydrogen-bond analysis demonstrated clear differences in the stability of ligand–CDK2 interactions over the 200 ns simulation (Figure 6). Ligand C62 exhibited the highest and most

persistent hydrogen-bonding profile, typically maintaining four to six bonds, indicating strong and sustained polar interactions within the binding pocket. While compound X4 similarly formed frequent hydrogen bonds, X3, X6, and X7 showed fewer and more transient interactions. Doxorubicin maintained only one to three hydrogen bonds, reflecting comparatively weaker polar stabilization.

Based on the integrated evaluation of RMSD, RMSF, radius of gyration, and hydrogen-bonding profiles, it demonstrated the most favorable overall stability among the designed ligands. All Hydroxyxanthones maintained consistently low RMSD values, induced minimal fluctuations within the critical 18–150 binding region, and preserved a stable global protein compactness throughout the simulation.

The MM/PBSA results align well with the molecular dynamics findings and collectively provide a comprehensive picture of ligand performance. Compound X4 exhibits the most favorable binding free energy (–20.27 kcal/mol), driven by strong van der Waals and electrostatic contributions, which is consistent with its frequent hydrogen-bonding interactions observed during the MD simulations. Compounds X3 and X7 show intermediate behavior, with moderate MD stability parameters and correspondingly moderate MM/PBSA energies. Collectively, these results indicate that X4 possesses the strongest thermodynamic affinity for CDK2.

The RMSD analyses provide clear insight into the dynamic stability of the designed EGFR inhibitors during the 200-ns simulation. The ligand-to-ligand RMSD profiles show that all four designed compounds (X2, X3, X5, and X7) maintain low internal fluctuations, generally below 1.5 Å, indicating strong conformational stability and minimal intramolecular distortion upon binding (Figure 7a). In contrast, Erlotinib exhibits greater internal flexibility, and Doxorubicin shows substantial structural fluctuations, reflecting poor geometric compatibility with the EGFR binding pocket. The ligand to backbone RMSD further highlights the differences in binding stability among the compounds (Figure 7b). Compound X5 demonstrates the most stable binding profile, consistently maintaining low positional deviation relative to the protein backbone, and in some regions performing comparably to or better than Erlotinib. Compounds X2, X3, and X7 also achieve stable binding modes with controlled fluctuations. Doxorubicin exhibits the greatest drift, underscoring its lack of compatibility with EGFR.

The docking results showed that position ligand interactions within EGFR residues 690–850, the RMSF profiles across this region offer a direct assessment of binding-induced stabilization (Figure 8a). Compounds X3, X5, and X7 elicit moderate and well-controlled fluctuations, indicating stable interactions with the binding site, whereas X2 induces notably higher mobility. Erlotinib maintains low fluctuations as expected for a well-characterized EGFR inhibitor, while the minimal RMSF observed for Doxorubicin likely reflects limited binding rather than true stabilization. The radius of gyration analysis shows that all EGFR–ligand complexes reach stable compactness after the initial equilibration phase (Figure 8b). Among the designed compounds, X3 and X7 maintain Rg values comparable to Erlotinib, indicating effective preservation of global structural integrity. X5 exhibits slightly higher variability yet remains stable overall, whereas X2 induces larger early fluctuations, reflecting weaker structural stabilization. Doxorubicin displays the lowest Rg values, likely due to minimal engagement with the binding site rather than true stabilizing effects.

The hydrogen-bond analysis shows that the designed ligands form consistent polar interactions with EGFR throughout the 200-ns simulation (Figure 9). Compound X5 exhibits the most frequent H-bonds, indicating strong stabilizing contacts within the binding pocket, while X2, X3, and X7 maintain intermittent but recurrent interactions. In contrast, Erlotinib forms fewer hydrogen bonds, and Doxorubicin shows only sporadic contacts. Overall, the designed ligands, particularly X5, demonstrate superior stability during the simulation.

The MMPBSA binding energies reinforce the trends observed in the MD simulations (Table 4). Compound X7 (–25.96 kcal/mol) and X5 (–23.13 kcal/mol) display the most favorable binding among the designed ligands, consistent with their stable RMSD, compact Rg profiles, and persistent hydrogen bonding. Ligands X3 and X2, with weaker energies (–14.49 and –12.93 kcal/mol), correspondingly show greater structural fluctuations and reduced stability during simulation. Erlotinib exhibits the strongest binding energy (–32.30 kcal/mol), in line with its known high affinity and stable MD behavior, whereas Doxorubicin, despite a moderate value (–21.84 kcal/mol), shows limited stabilizing interactions and poorer dynamic compatibility. Collectively, the data highlight X5 and X7 as the most promising EGFR inhibitors among the designed compounds.

Based on the Lipinski's rule of five, the drug candidate needs to possess the requisite physicochemical characteristics, which include the following: molecular weight <500 daltons, the logarithm of the octanol-water partition coefficient (log P) <5, rotatable bonds (ROTB) <10, hydrogen bond acceptor (HBA) <10, hydrogen bond donor (HBD) <5, and polar surface area (PSA) <140 Å [38]. All compounds meet those parameters. However, only compound X7 is unsuitable for the parameter of polar surface area.

The assessment of the pharmacokinetic properties of compounds X2, X3, X5, and X7 is essential to evaluate potential absorption, distribution, metabolism, excretion, and toxicity. In the absorption parameter, the Caco-2 model serves as a widely adopted in vitro representation of the human mucosa, playing a crucial role in the prediction of oral medication absorption. A pharmaceutical candidate is deemed to possess substantial Caco-2 permeability if its performance exceeds a value of 0.90 [39]. The Caco-2 permeability values of compounds X3 and X7 have exceeded the acceptable threshold. The Intestinal Absorption (IA) parameter denotes the portion of the drug that is absorbed by the human intestine. An absorption rate of 80% is considered favorable, while a rate below 30% is seen as unfavorable [40]. The IA values of all compounds surpassed 80%, signifying their appropriateness for absorption in the human intestine.

The distribution of hydroxyxanthone derivatives was quantified using the volume distribution (VDss). This parameter reflects the total quantity of a drug present in the body and is associated with a low value (log VDss <- 0.15) [41]. Compounds X3 and X7 exhibited a VDss value of less than -0.15, signifying their lower distribution in tissue compared to plasma [42, 43]. Afterward, the determination of BBB permeability explains how drugs pass through the blood-brain barrier. Molecules that have a logBB exceeding 0.3 are easily taken in by the brain, whereas those with a logBB lower than -1 are not effectively distributed to the brain [44]. Another approach involves the blood-brain permeability-surface area product (logPS), also recognized as Central Nervous System (CNS) permeability [45]. The LogPS value higher than -2 suggests penetration into the CNS, while a LogPS value lower than -3 suggests that it is not able to reach the CNS. Compound X3 exhibits the ability to readily permeate both the blood-brain barrier and the central nervous system, as evidenced by its BBB and CNS values.

The results of the metabolism parameters indicate that the hydroxyxanthones were found to be unsuitable as substrates for CYP2D6 and CYP3A4. It is also noteworthy that these compounds did not exhibit inhibitory activity against these specific substrates. These two substrates are particularly essential for the metabolism of Cytochrome P450. Cytochrome P450 is a crucial detoxifying enzyme found primarily in the human liver [46]. Moreover, the excretion characteristics suggested that each of the compounds X2, X3, X5, and X7 revealed a total clearance value within the range of 0.039 to 0.357. However, it's important to note that these compounds did not meet the criteria for Renal Organic Cation Transporter 2 (OCT2) parameters. The OCT2 parameter is significant as it relates to the drug's disposition and clearance [47].

The toxicity analysis revealed that all hydroxyxanthone derivatives (X2, X3, X5, and X7) exhibited mutagenic potential in the AMES test and showed inhibitory activity toward hERG II, indicating possible cardiotoxic risk through potassium channel blockade leading to long QT syndrome. Although the maximum tolerated dose values suggested low overall toxicity, these findings highlight critical safety concerns. Despite X7 demonstrating the most favorable docking and MD results, its potential as a drug candidate should be approached with caution. Accordingly, X7 is better regarded as a promising in silico lead requiring further optimization to mitigate mutagenic and cardiotoxic risks. Future studies should include confirmatory AMES and hERG assays, metabolite analysis, and structure–activity-based modifications. Additionally, hepatotoxicity predictions were negligible for X2 and X3, and none of the derivatives were associated with skin sensitization effects.

In conclusion, the comprehensive in silico investigation integrating molecular docking, molecular dynamics simulations, MM-PBSA free energy calculations, and ADMET profiling identified hydroxyxanthone X4, X5, and X7 as the most promising candidates, exhibiting strong and stable binding affinities toward both CDK2 and EGFR targets implicated in colorectal cancer pathogenesis. Nonetheless, the predicted mutagenic potential and hERG II inhibitory activity necessitate cautious interpretation and underscore the need for structural refinement to mitigate these liabilities. Accordingly, hydroxyxanthones X4, X5, and X7 should be regarded as a lead compound for further optimization and subjected to rigorous in vitro and in vivo validation to substantiate its therapeutic efficacy and safety profile.

Author Contribution Statement

All authors contributed equally in this study.

Acknowledgements

None.

Conflict of Interest

None.

References

1. Sung H, Ferlay J, Siegel RL, Laversanne M, Soerjomataram I, Jemal A, et al. Global cancer statistics 2020: Globocan estimates of incidence and mortality worldwide for 36 cancers in 185 countries. CA Cancer J Clin. 2021;71(3):209-49. https://doi.org/10.3322/caac.21660.
2. Xi Y, Xu P. Global colorectal cancer burden in 2020 and projections to 2040. Transl Oncol. 2021;14(10):101174. https://doi.org/10.1016/j.tranon.2021.101174.
3. Siegel RL, Miller KD, Jemal A. Cancer statistics, 2017. CA Cancer J Clin. 2017;67(1):7-30. https://doi.org/10.3322/caac.21387.
4. Pan DC, Krishnan V, Salinas AK, Kim J, Sun T, Ravid S, et al. Hyaluronic acid-doxorubicin nanoparticles for targeted treatment of colorectal cancer. Bioeng Transl Med. 2021;6(1):e10166. https://doi.org/10.1002/btm2.10166.
5. Banerjee S, Nau S, Hochwald SN, Xie H, Zhang J. Anticancer properties and mechanisms of botanical derivatives. Phytomedicine Plus. 2023;3(1):100396. https://doi.org/https://doi.org/10.1016/j.phyplu.2022.100396.
6. Çankaya N, Yalçin S. Antiproliferative activity and interaction with proteins of n-cyclohexylacrylamide. Saudi J Biol Sci. 2022;29(11):101670. https://doi.org/10.1016/j.sjbs.2020.04.030.
7. Wood DJ, Korolchuk S, Tatum NJ, Wang LZ, Endicott JA, Noble MEM, et al. Differences in the conformational energy landscape of cdk1 and cdk2 suggest a mechanism for achieving selective cdk inhibition. Cell Chem Biol. 2019;26(1):121-30.e5. https://doi.org/10.1016/j.chembiol.2018.10.015.
8. Susanti R, Dafip M, Mustikaningtyas D, Putra A. Predictive action of oncomir in suppressing tp53 signaling pathway in hypoxia-conditioned colon cancer cell line hct-116. Cell Biol Int. 2024;48(12):1891-905. https://doi.org/10.1002/cbin.12243.
9. Abrahams B, Gerber A, Hiss DC. Combination treatment with egfr inhibitor and doxorubicin synergistically inhibits proliferation of mcf-7 cells and mda-mb-231 triple-negative breast cancer cells in vitro. Int J Mol Sci. 2024;25(5). https://doi.org/10.3390/ijms25053066.
10. Piawah S, Venook AP. Targeted therapy for colorectal cancer metastases: A review of current methods of molecularly targeted therapy and the use of tumor biomarkers in the treatment of metastatic colorectal cancer. Cancer. 2019;125(23):4139-47. https://doi.org/10.1002/cncr.32163.

11. Mazur G, Pańczyk-Straszak K, Waszkielewicz AM. Xanthone derivatives in the fight against glioblastoma and other cancers. Applied Sciences. 2023;13(5):2897.
12. Kurniawan YS, Fatmasari N, Pranowo HD, Sholikhah EN, Jumina J. Investigation on anticancer agent against cervical and colorectal cancer cell lines: One-pot synthesis, in vitro and in silico assays of xanthone derivatives. J Appl Pharm Sci. 2024;14(3):145-53. https://doi.org/ 10.7324/japs.2024.160049.
13. Kurniawan YS, Priyangga KTA, Jumina, Pranowo HD, Sholikhah EN, Zulkarnain AK, et al. An update on the anticancer activity of xanthone derivatives: A review. Pharmaceuticals (Basel). 2021;14(11). https://doi.org/10.3390/ph14111144.
14. Miladiyah I, Jumina J, Haryana SM, Mustofa M. Biological activity, quantitative structure-activity relationship analysis, and molecular docking of xanthone derivatives as anticancer drugs. Drug Des Devel Ther. 2018;12:149-58. https://doi.org/10.2147/dddt.S149973.
15. Su QG, Liu Y, Cai YC, Sun YL, Wang B, Xian LJ. Anti-tumour effects of xanthone derivatives and the possible mechanisms of action. Invest New Drugs. 2011;29(6):1230-40. https://doi.org/10.1007/s10637-010-9468-5.
16. Fatmasari N, Kurniawan YS, Jumina J, Anwar C, Priastomo Y, Pranowo HD, et al. Synthesis and in vitro assay of hydroxyxanthones as antioxidant and anticancer agents. Sci Rep. 2022;12(1):1535. https://doi.org/10.1038/s41598-022-05573-5.
17. Pettersen EF, Goddard TD, Huang CC, Couch GS, Greenblatt DM, Meng EC, et al. Ucsf chimera--a visualization system for exploratory research and analysis. J Comput Chem. 2004;25(13):1605-12. https://doi.org/10.1002/jcc.20084.
18. Hanwell MD, Curtis DE, Lonie DC, Vandermeersch T, Zurek E, Hutchison GR. Avogadro: An advanced semantic chemical editor, visualization, and analysis platform. J Cheminform. 2012;4(1):17. https://doi.org/10.1186/1758-2946-4-17.
19. Neese F. Software update: The ORCA program system Version 5.0. Wiley Interdisciplinary Reviews: Comput Mol Sci. 2022;12(5):e1606.
20. 20. Morris GM, Huey R, Lindstrom W, Sanner M.F, Belew RK, Goodsell DS, et al. Autodock4 and autodocktools4: Automated docking with selective receptor flexibility. J Comput Chem. 2009;30(16):2785–91. Https://doi.Org/10.1002/jcc.21256digital
21. Mukesh B, Rakesh K. Molecular docking: a review. Int J Res Ayurveda Pharm. 2011 Jan 1;2(6):1746-51.
22. Fuhrmann J, Rurainski A, Lenhof HP, Neumann D. A new lamarckian genetic algorithm for flexible ligand-receptor docking. J Comput Chem. 2010;31(9):1911-8. https://doi.org/10.1002/jcc.21478.
23. Biovia DS. Discovery studio visualizer. San Diego: 2019.
24. Hess B, Kutzner C, van der Spoel D, Lindahl E. Gromacs 4: Algorithms for highly efficient, load-balanced, and scalable molecular simulation. J Chem Theory Comput. 2008;4(3):435-47. https://doi.org/10.1021/ct700301q.
25. Huang J, MacKerell AD, Jr. Charmm36 all-atom additive protein force field: Validation based on comparison to nmr data. J Comput Chem. 2013;34(25):2135-45. https://doi.org/10.1002/jcc.23354.
26. Pronk S, Páll S, Schulz R, Larsson P, Bjelkmar P, Apostolov R, et al. Gromacs 4.5: A high-throughput and highly parallel open source molecular simulation toolkit. Bioinformatics. 2013;29(7):845-54. https://doi.org/10.1093/bioinformatics/btt055.
27. Verlet L. Computer "experiments" on classical fluids. I. Thermodynamical properties of lennard-jones molecules. Phys Rev. 1967;159(1):98-103. https://doi.org/10.1103/PhysRev.159.98.
28. Hünenberger PH. Thermostat algorithms for molecular dynamics simulations. Adv Polym Sci. 2005;173:105-49. Https://doi.Org/10.1007/b99427.
29. Martoňák R, Laio A, Parrinello M. Predicting crystal structures: The parrinello-rahman method revisited. Phys Rev Lett. 2003;90(7):075503. https://doi.org/10.1103/PhysRevLett.90.075503.
30. Kumari R, Kumar R, Lynn A. G_mmpbsa--a gromacs tool for high-throughput mm-pbsa calculations. J Chem Inf Model. 2014;54(7):1951-62. https://doi.org/10.1021/ci500020m.
31. Vifta RL, Yanti S, Suyudi SD, Susmayanti W. Insight into the biological activity of zingiber officinale var. Amarum extract as antioxidant and sars-cov-2 inhibitor in-silico. Trop. J Nat Prod Res. 2025;9(3):1097-104. https://doi.org/10.26538/tjnpr/v9i3.26.
32. Pires DE, Blundell TL, Ascher DB. Pkcsm: Predicting small-molecule pharmacokinetic and toxicity properties using graph-based signatures. J Med Chem. 2015;58(9):4066-72. https://doi.org/10.1021/acs.jmedchem.5b00104.
33. Ramírez D, Caballero J. Is it reliable to take the molecular docking top scoring position as the best solution without considering available structural data? Molecules. 2018;23(5). https://doi.org/10.3390/molecules23051038.
34. Odhar HA, Hashim AF, Ahjel SW, Humadi SS. Molecular docking and dynamics simulation analysis of the human fxiia with compounds from the mcule database. Bioinformation. 2023;19(2):160-6. https://doi.org/10.6026/97320630019160.
35. De Bondt HL, Rosenblatt J, Jancarik J, Jones HD, Morgan DO, Kim SH. Crystal structure of cyclin-dependent kinase 2. Nature. 1993;363(6430):595-602. https://doi.org/10.1038/363595a0.
36. Roskoski R, Jr. Cyclin-dependent protein kinase inhibitors including palbociclib as anticancer drugs. Pharmacol Res. 2016;107:249-75. https://doi.org/10.1016/j.phrs.2016.03.012.
37. Yuliana A, Rahmiyani I, Kartika C. Molecular docking and molecular dynamics simulation using monascus sp. As a candidate cervical cancer drug. J Trop Pharm. Chem. 2023;7(1):41-51. https://doi.org/ 10.25026/jtpc.V7i1.432.
38. Moreau Bachelard C, Coquan E, du Rusquec P, Paoletti X, Le Tourneau C. Risks and benefits of anticancer drugs in advanced cancer patients: A systematic review and meta-analysis. EClinicalMedicine. 2021;40:101130. https://doi.org/10.1016/j.eclinm.2021.101130.
39. Lipinski CA. Lead- and drug-like compounds: The rule-of-five revolution. Drug Discov Today Technol. 2004;1(4):337-41. https://doi.org/10.1016/j.ddtec.2004.11.007.
40. Sambuy Y, De Angelis I, Ranaldi G, Scarino ML, Stammati A, Zucco F. The caco-2 cell line as a model of the intestinal barrier: Influence of cell and culture-related factors on caco-2 cell functional characteristics. Cell Biol Toxicol. 2005;21(1):1-26. https://doi.org/10.1007/s10565-005-0085-6.
41. Radchenko EV, Dyabina AS, Palyulin VA, Zefirov NS. Prediction of human intestinal absorption of drug compounds. Russ Chem Bull. 2016 Feb;65(2):576-80.
42. Trott O, Olson AJ. Autodock vina: Improving the speed and accuracy of docking with a new scoring function, efficient optimization, and multithreading. J Comput Chem. 2010;31(2):455-61. https://doi.org/10.1002/jcc.21334.
43. Flores-Holguín N, Frau J, Glossman-Mitnik D. Computational pharmacokinetics report, admet study and conceptual dft-based estimation of the chemical reactivity properties of marine cyclopeptides. ChemistryOpen. 2021;10(11):1142-9. https://doi.org/10.1002/open.202100178.

44. Kunwittaya S, Nantasenamat C, Treeratanapiboon L, Srisarin A, Isarankuram C, Pachayasittikul V. Influence of logbb cut-off on the predicton of blood brain barrier permeability. Biomed Appl Tech J. 2013;1:16-34.
45. Cornelissen FMG, Markert G, Deutsch G, Antonara M, Faaij N, Bartelink I, et al. Explaining blood-brain barrier permeability of small molecules by integrated analysis of different transport mechanisms. J Med Chem. 2023;66(11):7253-67. https://doi.org/10.1021/acs.jmedchem.2c01824.
46. Zhao M, Ma J, Li M, Zhang Y, Jiang B, Zhao X, et al. Cytochrome p450 enzymes and drug metabolism in humans. Int J Mol Sci. 2021;22(23). https://doi.org/10.3390/ijms222312808.
47. Couroussé T, Gautron S. Role of organic cation transporters (octs) in the brain. Pharmacol Ther. 2015;146:94-103. https://doi.org/10.1016/j.pharmthera.2014.09.008.